RESEARCH ARTICLE
doi: 10.2306/scienceasia1513-1874.2023.s007

ScienceAsia 49S (2023): **32–42**

Effect of isothermal heat treatment on microstructure and wear behavior of pearlitic rail steel

Nattaya Tosangthum[a], **Rungtip Krataitong**[a], **Ruangdaj Tongsri**[a], **Amporn Wiengmoon**[b,*]

[a] MTEC, National Science and Technology Development Agency (NSTDA), Pathum Thani 12120 Thailand
[b] Department of Physics, Faculty of Science, Naresuan University, Phitsanulok 65000 Thailand

*Corresponding author, e-mail: ampornw@nu.ac.th

Received 18 Jan 2023, Accepted 31 Aug 2023
Available online 27 Dec 2023

ABSTRACT: The properties of pearlitic steel are controlled by pearlite characteristics, which in turn depend on transformation temperatures. This work aims to study the relationship between the microstructure, hardness, and wear behavior of pearlitic rail steel obtained via different heat treatment conditions. The samples were austenitized at temperatures in the range of 800–1000 °C and then subjected to isothermal treatment at temperatures of 400–600 °C. The microstructure was examined using optical microscopy and scanning electron microscopy. Sample hardness was measured using Vickers microhardness tester. Pin-on-disc testing was used to study the wear behavior of samples. The results showed that the austenite grain size increased with increasing austenitization temperatures. The heat-treated microstructures contained proeutectoid ferrite, bainitic ferrite, and pearlite. Pearlite colony size and interlamellar spacing increased with increasing isothermal temperatures. The hardness of the rail material increased when the microstructural scale was refined. In addition to the hardness, the type and morphology of phases in the sample microstructure strongly influenced the wear behavior. The important wear mechanisms included fatigue cracking, delamination, and adhesive wear.

KEYWORDS: pearlitic rail, microstructure, wear resistance, isothermal heat treatment

INTRODUCTION

The rail industry has been focusing on improving the materials by increasing hardness and changing microstructures to accommodate modern rail systems that require higher speeds and larger axle loads. One goal of rail material developments is to reduce the wear rate. Pearlitic steel still shows its importance for railroad tracks due to its excellent mechanical properties, wear resistance, and rolling contact fatigue (RCF) resistance. Moreover, it is superior to bainitic steel in terms of wear resistance [1]. Since pearlitic steel is the most widely used as prime rail materials, its properties still need to be further studied and improved.

The strength of a full pearlitic steel is highly dependent on the spacing between cementite lamellae known as interlamellar spacing [2, 3]. The reduction of pearlite interlamellar spacing in steels could also increase resistance to sliding wear [4]. To get finer interlamellar spacing in pearlite, refinement by using proper heat treatment is a common practice. Pearlite refinement can be achieved through the enhancement of the phase transformation driving force such as by adding alloying elements and modifying the cooling conditions [5].

Regarding the alloying element effect, Tashiro et al [6] have reported that the content of proeutectoid ferrite was reduced by 10 vol.% and the cementite structure was also changed by adding silicon (Si), manganese (Mn), and nickel (Ni), followed by the heat treatment adjustment. This resulted in deformability enhancement wear and RCF reduction in ferrite-pearlite steels. The alloying chromium (Cr) plays a significant role in improving the strength and toughness of the pearlitic steels by reducing the austenite grains and lamellar spacing. The silicon (Si) and carbon (C) additions could change the austenite decomposition products in Fe-Mo-Mn alloy steel [7]. Furthermore, the carbon content, cooling rate, and size of prior austenite grains are determinants of whether conventional ferrite or Widmanstätten ferrite will form [8–10]. Controlling these variables makes it possible to achieve the desired structure [11, 12].

The hardness and wear resistance of wheel and rail materials generally have no direct correlation [13, 14]. Wear resistance is directly related to the material resistance to plastic deformation [15]. Moreover, the addition of carbon and solid solution strengthening also improves the wear resistance of ferrite-pearlite steel. On the other hand, precipitation strengthening caused a decrease of wear resistance as reported by Zeng et al [16]. Many previous works focused on the effect of pearlite interlamellar spacing and pearlite morphology on wear resistance using various types of tribometers [17–19]. Bataev et al [19] have reported that the loss of plasticity is due to interlayer defects along the layer boundaries in Widmanstätten structures. Wear and RCF of pearlitic steel are affected by proeutectoid ferrite content, prior austenite grain size, pearlite colony size, cementite morphology, and pearlite interlamellar spacing, according to Shi et al [5] and Li et al [17]. Garnham and Davis [20] indicated that cracks initially occur along the deformed proeu-

Table 1 Austenite grain size (AGS), pearlite colony size, and interlamellar spacing of sample at different austenite (T_γ) and isothermal temperatures (T_{iso}).

Sample	T_γ (°C)	T_{iso} (°C)	AGS (μm)	Pearlite colony size (μm)	Interlamellar spacing (nm)
S1	800	500	30	3.6	105
S2	900	500	46	3.9	91
S3	1000	500	58	3.7	117
S4	900	400	–	3.7	89
S5	900	600	–	4.3	117

tectoid ferrite line, increasing wear. One of the most common test rigs is probably a ball on disk tester due to its simplicity and well-explained tribological heterogeneity [21, 22]. It can be used to screen materials after they have been designed to reduce costs. In addition, the pure sliding contact is known to be the same as the contact between the rail rim and the wheel flange occurring during turning and braking.

Aside from the composition, different heat treatment processes can alter the phases present in the microstructure of rail steels. The tribological performance influenced by the combination of these microstructures needs to be further studied. Therefore, the main objective of the present work is to study the influence of microstructures of R260 pearlitic rail steel caused by different isothermal treatments on the hardness and sliding wear resistance.

MATERIALS AND METHODS

Materials and heat treatments

The rail samples were cut from the new R260 rail head with dimensions of 50 mm × 50 mm and 20 mm thick. The nominal compositions of the R260 rail steel were 0.73 wt.% C, 0.35 wt.% Si, 1.05 wt.% Mn, and balance of Fe. The as-received samples were reheated from room temperature to austenite temperature and held for 1 h before being isothermally treated in a salt bath for 5 min, and then all samples were water quenched to room temperature. To examine the effects of austenite temperature (T_γ) on the austenite grain size, 3 samples (S1, S2, and S3 in Table 1) were austenitized at temperatures of 800, 900, and 1000 °C with the same isothermal temperature of 500 °C. To examine the effect of isothermal temperatures (T_{iso}) on the pearlite colony and interlamellar spacing, 3 samples (S2, S4, and S5 in Table 1) were subjected to austenitization at 900 °C, which gave the highest hardness and lowest wear rate, and isothermal treatments at temperatures of 400, 500, and 600 °C, according to the time-temperature-transformation (TTT) diagram of R260 [23], to obtain the pearlite and bainite structures.

Microstructure characterization

Specimens for optical microscopy (OM) and field emission scanning electron microscopy (FE-SEM) were prepared according to a metallography standard procedure, including cutting, grinding on silicon carbide papers, polishing with diamond pastes, and then etching with 2% Nital in ethanol. The microstructural observation was conducted using Axiolab 5, Zeiss OM, and Apreo S. Thermo Fisher Scientific FE-SEM operated at 20 kV. The sizes of the pearlite colony and austenite grain were measured using the linear intercept method [24]. The grain size of austenite was determined using ten optical micrographs at ×500 magnification, and grain boundaries were determined using the proeutectoid ferrite networks. A pearlite colony was characterized by the area, in which the pearlite lamellae had the same orientation. Five SEM images were selected at ×3000 magnification, and 3 straight lines were drawn in each image to measure the sizes of the pearlite colonies. The pearlite interlamellar spacing was measured by drawing a straight line normal to the direction of the pearlite lamellae and dividing the length of the line by the amount of cementite and ferrite intercepts in each sample under ×10000 magnification.

Hardness and wear testing

Vickers micro-hardness and pin-on-disc wear tests were conducted. Vickers micro-hardness testing was performed on polished specimens using a 50 gf load (HV0.5) for 15 indentations using a Jinan HV-1000. The average value was based on 10 different areas.

Wear tests were carried out under dry conditions using a pin-on-disc tribometer according to ASTM G-99. The machine had a loaded pin that was pressed against a horizontal rotating disc to simulate the slip region of the wheel-rail interaction. The friction coefficient was calculated by dividing the tangential force by the normal load. Dead weights were used to apply the normal load, while a load cell was used to measure the tangential force. Discs were machined to a diameter of 25 mm with a thickness of 5 mm. The rail discs were tested against WC-Co pins with a radius of 6 mm and a hardness of about 77 HRC. A constant load of 15 N was applied for all tests. Such a load was equivalent to a Hertzian contact pressure of 2.1 GPa, which was slightly higher than the actual wheel/rail contact pressure of approximately 1.8 GPa [1]. The sliding speed of 0.1 m/s and the wear track radius of 6 mm were set. The test was performed at room temperature of 25 °C. Prior to testing, the disc sample was polished using silicon carbide paper to obtain a surface with a roughness of about 0.1 μm. Then, it was ultrasonically cleaned using ethanol. During the tests, the friction coefficient was measured in real-time. The test was conducted 3 times for each condition. The wear track width measurement was observed using

SEM, and an equation specified in ASTM G-99 was used to calculate the wear volume loss of the disc. Afterwards, the calculated value was used to determine the wear rate and wear coefficient (k). After pin-on-disc tests, the worn surface was characterized using Inspect50 SEM-FEG.

RESULTS AND DISCUSSION

Microstructure characterization

Fig. 1 shows typical OM and SEM images of the rail samples after isothermal heat treatment. The microstructures of all samples comprised proeutectoid ferrite (PF), pearlite grain (lamellar mixture of ferrite and cementite), and some bainitic ferrite (BF) plates, which form on prior austenite grain boundaries (PAGBs). However, the bainitic transformation in S3 and S4 samples terminated and was followed by pearlitic transformation. Although, the isothermal temperature of 400 °C falls in the bainitic transformation field in the TTT diagram of R260 steel [23], bainitic transformation stasis occurs because of 2 reasons which are that (i) the isothermally treated Fe-C-Mn alloys commonly show reaction stasis at temperatures close to bainite start temperature (Bs) and (ii) the soaking time at an isothermal temperature is too short for slow bainitic transformation kinetics. Generally, when the temperature decreases below the austenitizing temperature (T_γ), the austenite transforms into pearlite, and the PF films are formed along PAGBs. During isothermal transformation in the salt bath at temperatures of 400–600 °C, pearlite colonies nucleate on the PF-austenite interfaces and then grow into the austenite grains. In this work, the prior austenite grain size (AGS) at room temperature could be determined due to the presence of PF networks, which enable the application of the linear intercept method. It was found that the average AGS values of the samples S1 (austenitized at 800 °C), S2 (austenitized at 900 °C), and S3 (austenitized at 1000 °C), all treated under the same isothermal temperature (T_{iso}) of 500 °C, were 30 µm, 46 µm, and 58 µm as shown in Table 1. The AGS increased with increasing austenitization temperature as observed in previous works [2, 17]. It can be seen from this figure that the austenitization temperature has a strong influence on the austenite gain size.

BF plates could be observed clearly next to some PAGBs as illustrated in Fig. 2. Most BF plates nucleated on PAGBs at the initial stage of isothermal transformation and then grew into austenite grains. Isothermally needle-like BF plates arranged in parallel to one another at a certain angle from the grain boundary [10]. It was found that needle-like BF plates could be easily found in the samples S3 (T_γ=1000 °C/T_{iso}=500 °C) and S4 (T_γ = 900 °C/T_{iso} = 400 °C) but hardly observed in samples S1 (T_γ = 800 °C/T_{iso} = 500 °C) and S2 (T_γ = 900 °C/T_{iso} = 500 °C). The sample S3 had AGS larger than that of the sample S4, and the sample S3 had BF fraction lower than that of the sample S4. This indicates that the austenitization temperature has influence on bainitic ferrite transformation. A previous work [25] provided the same information related to the effect of austenitization temperature on bainitic transformation.

The effect of AGS on pearlite colony size and interlamellar spacing was also investigated as shown in Fig. 3. The AGS, pearlite colony size, and interlamellar spacing of the sample S1 (T_γ = 800 °C/T_{iso} = 500 °C) were 30 µm, 3.6 µm, and 105 nm, respectively, and those of the sample S3 (T_γ = 1000 °C/T_{iso} = 500 °C) were 80 µm, 3.7 µm, and 117 nm, respectively. Pearlite colony size and interlamellar spacing tend to increase with increasing AGS. According to research by Kavishe et al [10], the transformation was delayed as AGS increased because fewer nucleating sites were present per unit volume. Aranda et al [2] reported that the small AGS promoted faster kinetics for pearlite formation. The faster kinetics in a small AGS were related to more abundant nucleation sites, but the pearlite interlamellar spacing did not depend on the AGS.

Besides, Fig. 4 and Table 1 show the effect of isothermal temperature on pearlite colony size and interlamellar spacing. The pearlite colony sizes of the samples S4 (T_γ = 900 °C/T_{iso} = 400 °C), S2 (T_γ = 900 °C/T_{iso} = 500 °C), and S5 (T_γ = 900 °C /T_{iso} = 600 °C) were 3.7 µm, 3.9 µm, and 4.3 µm, respectively. The size of the pearlite colony increased as the isothermal temperature increased. This is due to the increase in the driving force caused by the increase in undercooling. Larger undercooling (lower transformation temperature) accelerates the nucleation rate but leads to the growth restriction effect [5]. The discrepancy on the effect of heat treatment temperature on pearlite colony size was also reported. Li et al [17] found that pearlite colony size increased with decreasing isothermal temperatures.

The pearlite interlamellar spacings of the samples S4 (T_γ = 900 °C/T_{iso} = 400 °C), S2 (T_γ = 900 °C/T_{iso} = 500 °C), and S5 (T_γ = 900 °C/T_{iso} = 600 °C) were 89 nm, 91 nm, and 117 nm, respectively. The pearlite interlamellar spacing increased with increasing isothermal temperature as reported in previous works [2, 5, 17, 18]. As given above, larger undercooling (lower transformation temperature) accelerates the nucleation rate [5], and smaller pearlite interlamellar spacing is obtained. In other words, the pearlite interlamellar spacing is inversely proportional to undercooling.

Hardness and wear properties

The interrelationship between microstructure, hardness, and wear behavior was investigated. It was found that the hardness values of samples decreased

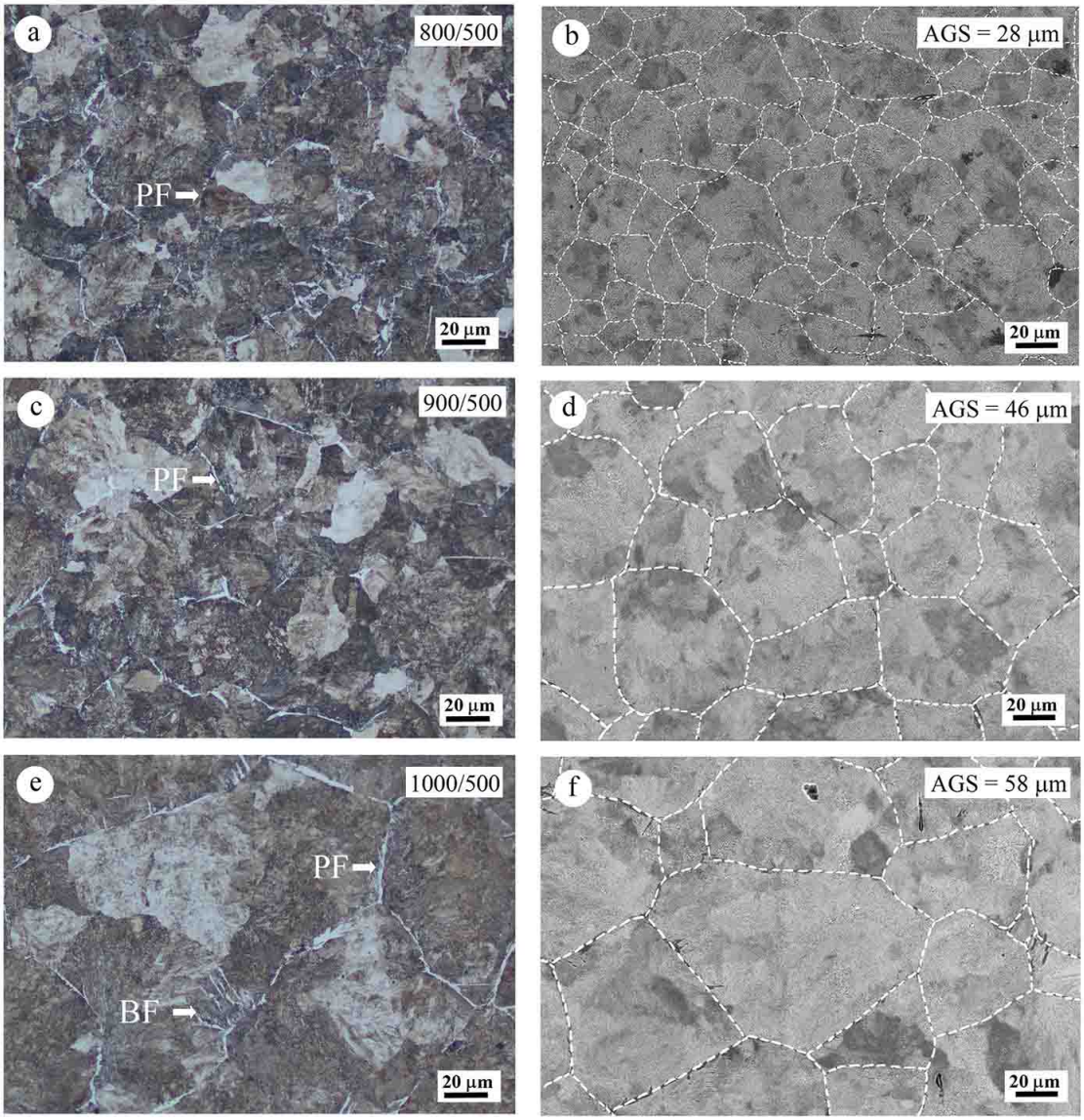

Fig. 1 OM and SEM images with the drawing line along the prior austenite grain of the S1, S2, and S3 samples obtained at an isothermal temperature of 500 °C and austenitization at different temperatures. (a–b) S1 at 800 °C, (c–d) S2 at 900 °C, and (e–f) S3 at 1000 °C.

Table 2 Hardness and wear parameter of experimental samples.

Sample	T_γ (°C)	T_{iso} (°C)	Hardness (HV0.5)	Wear rate (mm^3/m)	Wear coefficient	Friction coefficient
S1	800	500	393	3.32×10^{-4}	1.95×10^{-5}	0.58
S2	900	500	398	2.71×10^{-4}	1.59×10^{-5}	0.67
S3	1000	500	318	3.77×10^{-4}	2.21×10^{-5}	0.63
S4	900	400	418	3.64×10^{-4}	2.14×10^{-5}	0.61
S5	900	600	374	3.06×10^{-4}	1.95×10^{-5}	0.73

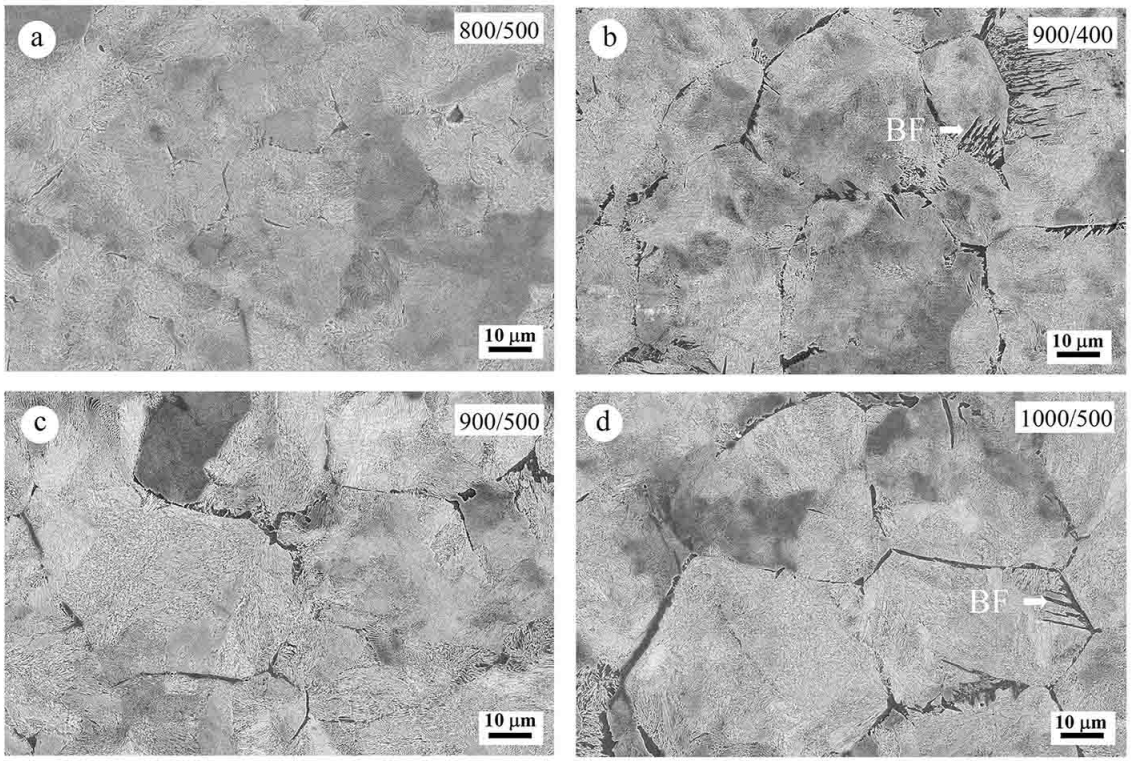

Fig. 2 SEM images showing the needle-like bainitic ferrite (BF) formed at the prior austenite grain boundaries at different austenitization and isothermal temperatures. (a) S1, (b) S4, (c) S2, and (d) S3.

from 393 HV0.5 to about 318 HV0.5 with increasing austenitization temperature (T_γ) from 800 °C to 1000 °C as shown in Table 2. This may be attributed to the increase of AGS and the presence of BF plates. Furthermore, the hardness values of samples also decreased from 418 HV0.5 to about 374 HV0.5 with the increase in the isothermal temperature (T_{iso}) from 400 °C to 600 °C. This is believed to be due to the increase in pearlite colony size and interlamellar spacing. Chaves et al [4] reported that the decrease in the pearlite formation temperature led to a reduction of the pearlite interlamellar spacing and increased hardness. Therefore, the hardness could be improved by decreasing the austenite grain size, pearlite colony size, and pearlite interlamellar spacing. The sample S4 exhibited the highest hardness, which may be attributed to the optimal austenite grain size and perlite structure, including the presence of BF plates.

The results of dry sliding tests on a pin-on-disk are given in Table 2. They showed the difference in material losses of R260 rail discs with different microstructures obtained via different treatment temperatures. The pin surface was unworn due to its high hardness. Therefore, the topography of the counter (pin) surface is not further discussed. Regarding the effect of different austenitization temperatures (under the same isothermal temperature of 500 °C), the steady wear rate of the sample austenitized at 900 °C (S2) showed the lowest value, followed by the sample austenitized at 800 °C (S1) and the sample austenitized at 1000 °C (S3), respectively. This is due to the narrowest interlamellar spacing in sample S2 compared to that of samples S1 and S3, although the AGS value of sample S2 is not the lowest one. Since there are insignificant differences in the pearlite colony sizes among the samples S1, S2, and S3, the effect of interlamellar spacing on the steady wear rate can be comfortably compared. This result conforms with the work of Li et al [17], who reported that pearlite interlamellar spacing has a more significant influence on the wear rate of rail material than AGS. Among the samples S1, S2, and S3, the wear rate tended to decrease with increasing hardness values. This behavior obeys the Archard relationship [4]. According to previous work [17], rolling/sliding testing was conducted on rail steel consisting of PF and pearlite phases. After testing, the elongated netted ferrite formed ferrite flowing lines by stretching in the direction of the tangential force. Due to its softness and relatively low yield limit, cracks are easy to form around it. The authors observed that plastic deformation becomes more severe as austenite grain size increases. These lead to accelerated crack

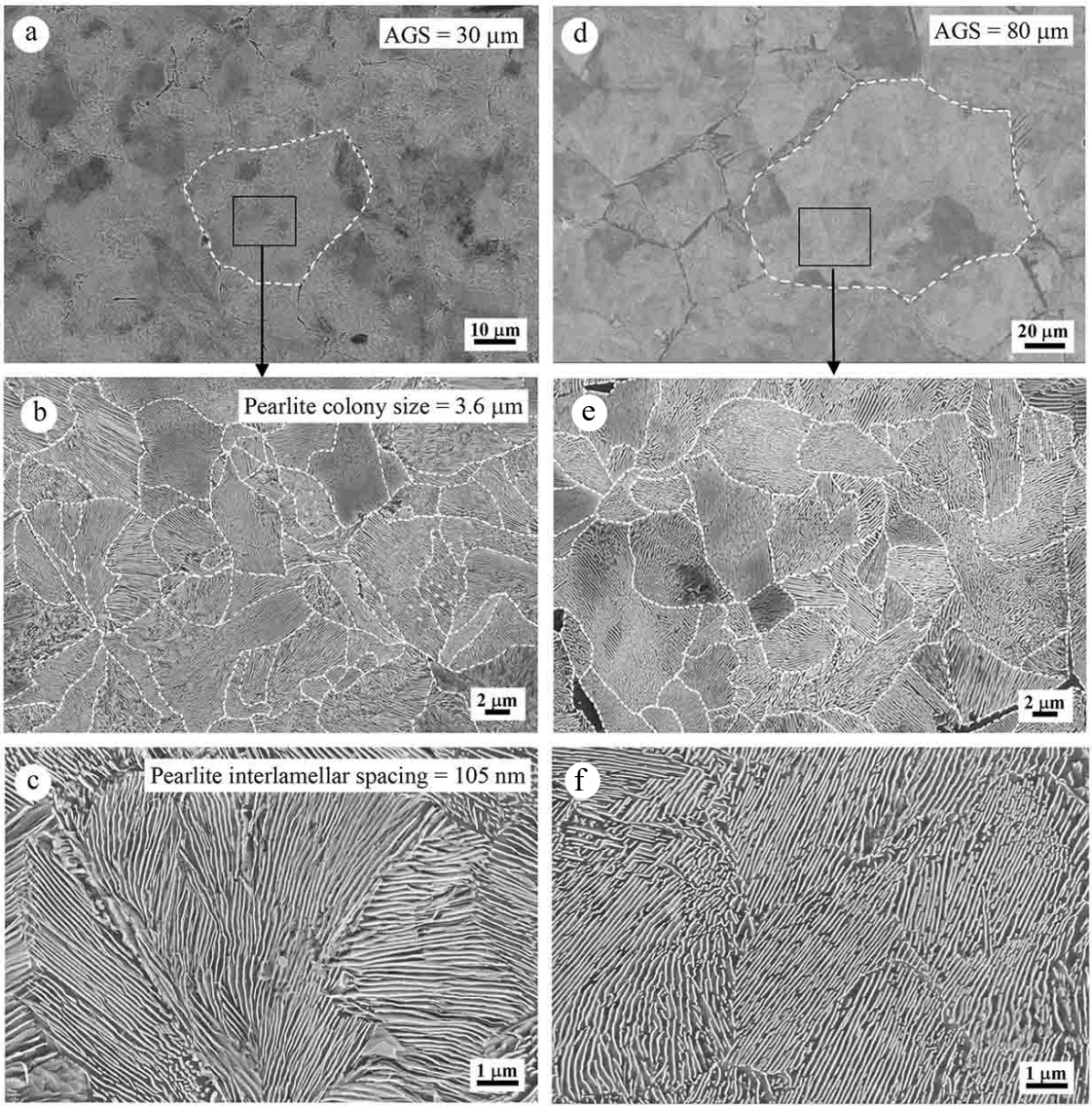

Fig. 3 SEM images showing the effect of AGS on pearlite colony size and the pearlite interlamellar spacing of the samples S1 and S3 obtained at different austenitization temperatures. (a–c) 800 °C and (d–f) 1000 °C. Fig. 3 (a and d) were obtained under × 1000 and × 500 magnifications, respectively.

initiation and growth. In another study, it was reported that mechanical property mismatches because of mixed microstructures in samples may cause high local stresses at the phase interface that contribute to crack initiation and propagation [26]. These reasons may contribute to a higher wear rate.

Regarding the effect of different isothermal temperatures (under the same austenitization temperature of 900 °C), the steady wear rate of the sample S2 (isothermally treated at 500 °C) showed the lowest value, followed by the samples S4 (isothermally treated at 400 °C) and S5 (isothermally treated at 600 °C), respectively. It was noticed that the sizes of pearlite scales (AGS, pearlite colony, and interlamellar spacing) of the samples S2 and S4 were almost the same, but the BF plates were found only in the sample S4. Although there was a finer pearlite structure in sample S4 than that in sample S5, the formation of a BF plate in the microstructure of sample S4 made the wear rate higher. This result confirms that a small amount of PF films and BF plates in a sample microstructure can lead to higher material loss due to dry sliding. As previously mentioned, a difference in the mechanical properties of mixed phases may accelerate the initiation and

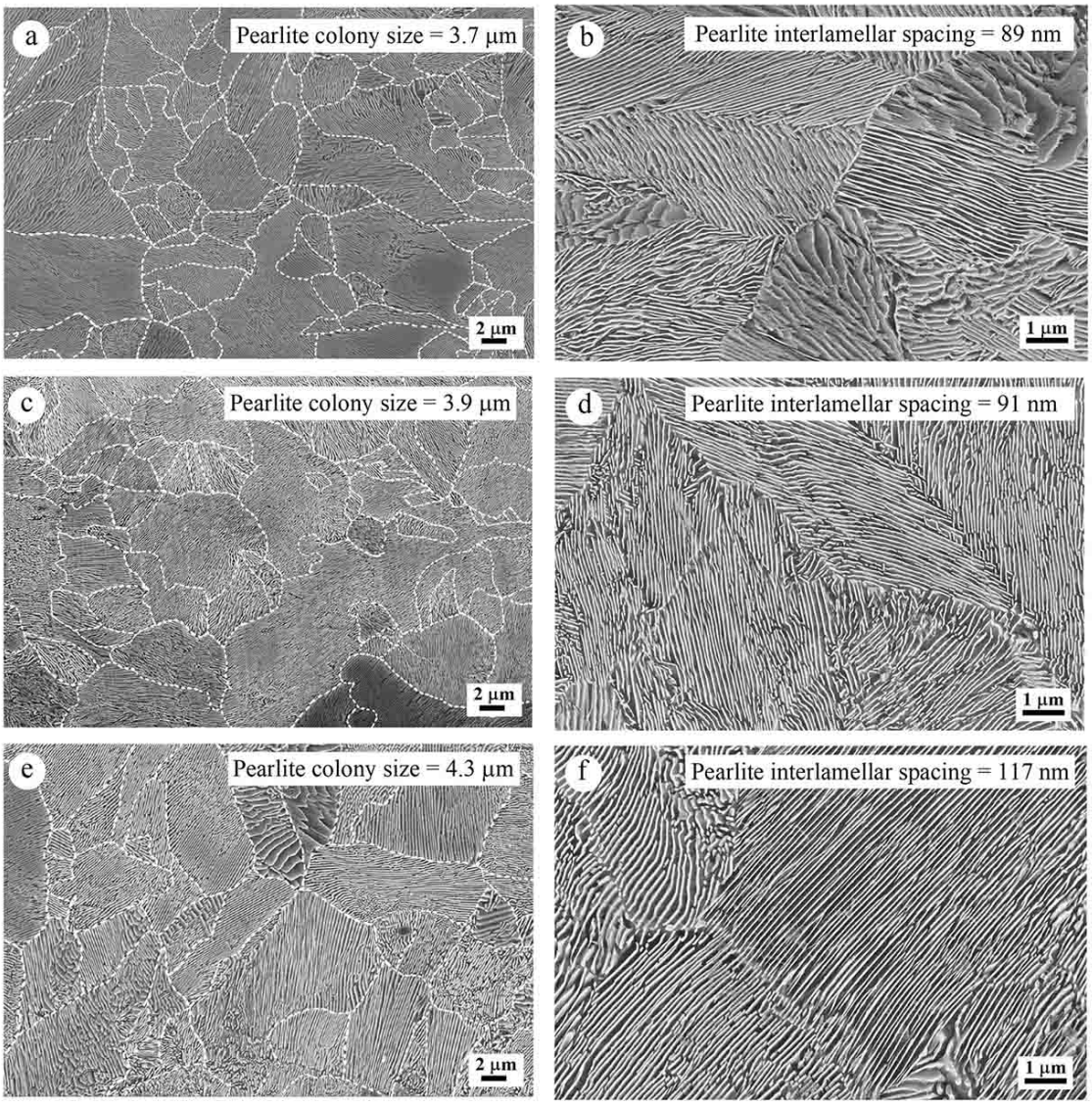

Fig. 4 SEM images showing the effect of isothermal temperature on pearlite colony size and the pearlite interlamellar spacing of samples S4, S2, and S5. (a–b) 400 °C, (c–d) 500 °C, and (e–f) 600 °C.

propagation of cracks [26]. The presence of BF plates leads to the loss of sample plasticity due to the weak boundary layer, which is the structural defect of the α phase [12]. It is established that crack propagation is mainly motivated by shearing and growth along the plastic flow. This is because the stress limit of the ferrite line is lower than that of fragmented pearlite [27, 28]. Both laboratory sliding testing by Lee et al [29] and field testing by Sawley et al [30] also found that pearlitic rail steel has much more significant work-hardening and surface hardness compared to bainitic steels, resulting in a lower wear rate. It was confirmed by Aleksandra et al [31] that the primary fatigue crack of the bainitic rail was propagated between the bainitic ferrite sheaves with different orientations. That is why full pearlite is best suited for rail materials. The sample S4 with the highest hardness exhibits the most wear, which may be due to the small size of the pearlite colony promoting cracking [32–35]. Moreover, the sample S4 microstructure contains PF films and BF plates, which increase crack-initiating sites. The results also indicate that initial hardness is not the only predictor of wear in pearlitic rail steel as given elsewhere [13, 15].

The wear tracks were analyzed via FE-SEM. The FE-SEM micrographs of the wear tracks on different heat-treated samples are shown in Fig. 5. Third body particles representing abrasive wear are observed in all

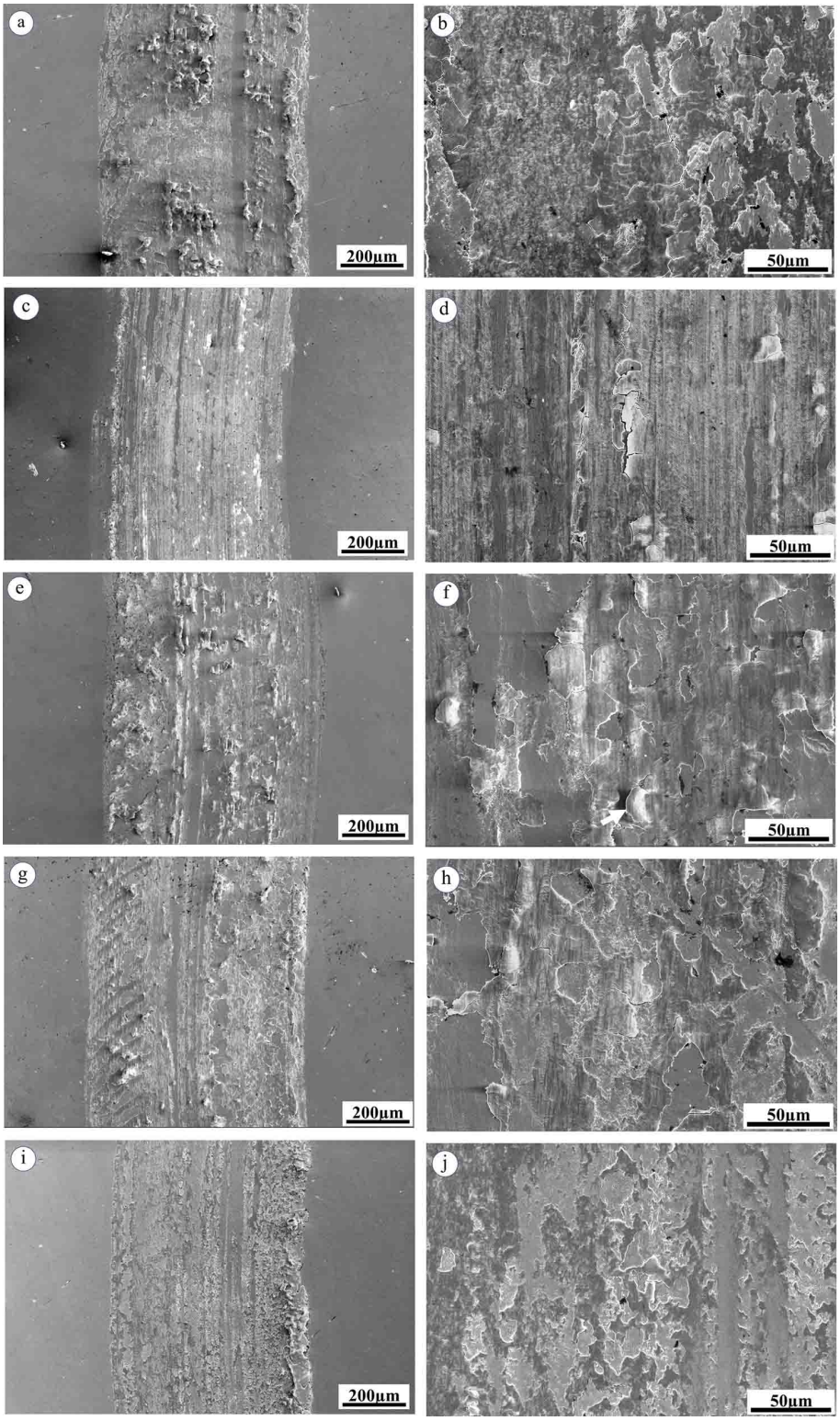

Fig. 5 SEM images of the worn track of samples at different austenitization and isothermal temperatures. (a–b) S1, (c–d) S2, (e–f) S3, (g–h) S4, and (i–j) S5.

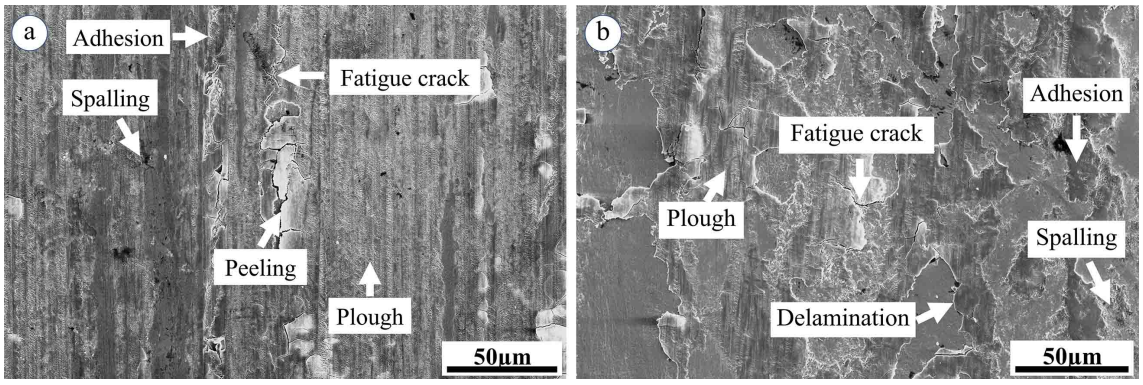

Fig. 6 SEM images showing the wear mechanism of the worn track of samples. (a) S2 and (b) S4.

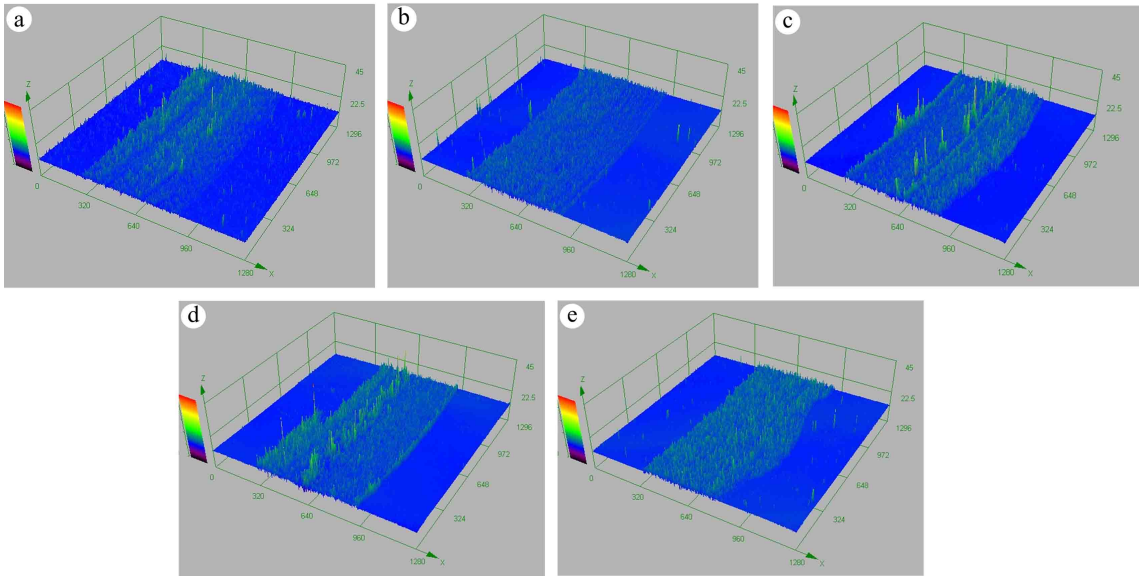

Fig. 7 Confocal laser scanning microscopy images of wear track after pin-on-disk test. (a) S1, (b) S2, (c) S3, (d) S4, and (e) S5.

wear tracks. In addition, severe adhesive wear was found to develop as a result of plastic deformation. The ploughing process causes plastic deformations. It has been widely reported that pearlitic steel used under rolling/sliding contact conditions showed a plastic deformation layer beneath the surface [22, 36–38]. In summary, damage mechanisms including fatigue cracks, adhesives, and delamination were observed in the wear tracks of heat-treated rail material samples. This is consistent with previous studies conducted on the wear of pearlite rail steels [39, 40]. The shear strain accumulation under cyclic loadings can cause the material to rupture after the critical limit has been reached. Strain along the shear bands forms a void/cavity that expands to cause surface cracking and then propagates, resulting in debris formation as flaking [28, 37, 39]. During testing, metal oxide was also observed. Friction between the contact zones causes a temperature increase, resulting in oxide debris that forms a layer on the worn track surface. This results in a change of overall friction behavior by reducing metal wear and keeping the system in a mild wear regime [40]. However, the aspect of the friction coefficient needs to be further demonstrated. Generally, the ductile phase, ferrite, promoted adhesion, and spalling increased material loss [38, 39]. Although ferrite is more ductile, it reaches its ductility limit first, resulting in a lower work hardening rate than pearlite during testing [36, 38]. According to Tosangthum et al [41], there is evidence proving that voids caused by rolling/sliding contact loading occur in the plastic deformation layer and exist at PF and ferrite/broken cementite interfaces. Besides, the surface damage of pearlitic-ferritic steel is spalling and mainly particle adhesion when compared with fully pearlitic steel.

As seen in Fig. 5(c,d), the wear track of the sample S2 showed more plastic ploughing with fewer fatigue cracks. In addition, the adhered particle, consisting of agglomerated debris, is small as shown in Fig. 5b. This may indicate a lower wear rate of the sample S2 as a result of higher work hardening due to the narrow lamellar spacing. Chaves et al [4] and Junjie et al [42] claimed that smaller lamellar spacing in pearlite increases plastic deformation ability, resulting in a decreased wear rate. The work hardening degree increased since the thin cementite lamellar was hardly broken in a rolling direction and also because many dislocations were piling up in the ferrite phase. As shown in Fig. 6, sample S4, which has a higher wear rate, has a damaged surface with larger cracks and detachments when compared to those of sample S2, which has a lower wear rate. Both of them have microstructures that are almost the same size, but BF is only present in sample S4. Therefore, as previously mentioned, it is possible that BF may accelerate crack initiation and growth [12].

Wear tracks were also observed using confocal microscopy techniques as can be seen in Fig. 7. Higher green peaks on the track of samples S1 (Fig. 7a), S3 (Fig. 7c), and S4 (Fig. 7d) indicate greater adhesion build-up than those of samples S2 (Fig. 7b) and S5 (Fig. 7e). The wear tracks observed by confocal microscopy are consistent with the SEM images shown in Fig. 5 and the value of wear rate shown in Table 2. This result agrees with the previous work by Li et al [38], which reported that PF can promote fatigue cracking and adhesion and increase material loss when samples are tested under rolling/sliding. To confirm whether proeutectoid ferrite accelerates fatigue damage, further investigation is needed for this work because, in addition to the composition and mechanical characteristics of the material, many other factors such as testing conditions, counterpart material, and surface roughness can affect wear properties.

CONCLUSION

The present study found that the increase of austenitization temperature from 800 °C to 1000 °C increased AGS from 28 µm to 58 µm. The pearlite colony size was increased from 3.7 µm to 4.3 µm, and the pearlite interlamellar spacing was increased from 89 nm to 117 nm with the increase in the isothermal temperature from 400 °C to 600 °C. On the other hand, the hardness decreased with increasing austenitization and isothermal temperatures. The hardness could be improved by decreasing AGS, pearlite colony size, and pearlite interlamellar spacing. Maximum hardness could be obtained after austenitization at 900 °C, followed by an isothermal at 400 °C. Besides the microstructural scales of pearlite, PE and BF also affected the wear mechanism and wear rate. The minimum wear rate was obtained by austenitization at 900 °C, followed by an isothermal at 500 °C.

Acknowledgements: This work was supported by Naresuan University, National Science, Research and Innovation Fund (NSRF) Grant number R2565B065 and Thailand National Metal and Materials Technology Center. The authors would like to thank Bangkok Expressway and Metro Public Company Limited for supporting R260 rail material.

REFERENCES

1. Lee KM, Polycarpou AA (2005) Wear of conventional pearlitic and improved bainitic rail steels. *Wear* **259**, 391–399.
2. Aranda MM, Kim B, Rementeria R, Capdevila C, García C, Andrés DE (2014) Effect of prior austenite grain size on pearlite transformation in a hypoeuctectoid Fe-C-Mn steel. *Metall Mater Trans A* **45**, 1778–1786.
3. Wang M, Zhang F, Yang Z (2017) Effects of high-temperature deformation and cooling process on the microstructure and mechanical properties of an ultrahigh-strength pearlite steel. *Mater Des* **114**, 102–110.
4. Chaves APG, Centeno DMA, Masoumi M, Goldenstein H (2020) Effect of the microstructure on the wear resistance of a pearlitic steel. *Mat Res* **23**, 1–8.
5. Shi X, Zhang X, Diao G, Wen Z, Jin XS, Yan Q (2022) Isothermal heat treatment of wheel steel with high Cr and Si contents based on microstructure, mechanical properties, and wear performance. *J Mater Eng Perform* **31**, 341–352.
6. Tashiro H, Sato H (1991) Effect of alloying elements on the lamellar spacing and the degree of regularity of pearlite in eutectoid steel. *J Japan Ins Metals* **55**, 1078–1085.
7. Srijampan W, Wiengmoon A, Nakornkaw P, Patcharawit T, Yotkaew T, Tosangthum N, Tongsri R (2021) Effects of silicon carbide contents on the microstructure of sintered steels. *ScienceAsia* **47**, 51–59.
8. Yi HL (2010) Full pearlite obtained by slow cooling in medium carbon steel. *Mat Sci Eng A* **527**, 7600–7604.
9. He W, Yinli C, Lan S, Di T (2018) Effect of cooling rate and isothermal temperature on the phase transformation and microstructure evolution in SWRH82B high high-carbon steel. *Mater Res Express* **5**, 086506.
10. Kavishe FPL, Baker TJ (2013) Effect of prior austenite grain size and pearlite interlamellar spacing on strength and fracture toughness of eutectoid rail steel. *Mater Sci Technol* **2**, 816–822.
11. Todorov RP, Khristov KG (2004) Widmanstätten structure of carbon steels. *Met Sci Heat Treat* **46**, 49–53.
12. Zhao S, Min N, Li W (2022) Formation of Widmanstätten ferrite and grain boundary ferrite in a hypereutectoid pearlitic steel. *Metals* **12**, 493.
13. Jha AK, Prasad BK, Modi OP, Das S, Yegneswaranm AH (2003) Correlating microstructural features and mechanical properties with abrasion resistance of a high strength low alloy steel. *Wear* **254**, 120–128.
14. Gunduz S, KacaR, Soykan H (2008) Wear behavior of forging steels with different microstructure during dry sliding. *Tribol Int* **41**, 348–355.
15. Wang Y, Lei T, Liu J (1999) Tribo-metallographic behavior of high carbon steels in dry sliding: II. Microstructure and wear. *Wear* **231**, 1–11.

16. Zeng D, Lu L, Zhang N, Gong Y, Zhang J (2016) Effect of different strengthening methods on rolling/sliding wear of ferrite-pearlite steel. *Wear* **358–359**, 62–71.
17. Li XC, Ding HH, Wang WJ, Guo J, Liu QY, Zhou ZR (2021) Investigation on the relationship between microstructure and wear characteristic of rail materials. *Tribol Int* **163**, 107152.
18. Herian J, Aniołek K (2010) Abrasive wear of railway sections of steel with a different pearlite morphology in railroad switches. *J Achiev Mater Manuf Eng* **43**, 236–243.
19. Bataev IA, Bataev AA, Burov VG, Lizunkova YS, Zakharevich EE (2008) Structure of Widmanstätten crystals of ferrite and cementite. *Steel Transl* **38**, 684–687.
20. Garnham JE, Davis CL (2008) The role of deformed rail microstructure on rolling contact fatigue initiation. *Wear* **265**, 1363–1372.
21. Faccoli M, Petrogalli C, Ghidini A (2017) A pin-on-disc study on the wear behaviour of two high-performance railway wheel steels. *Tribol Lett* **65**, 152.
22. Shariff SM, Pal TK, Padmanabham G, Joshi SV (2011) Comparative study on dry sliding wear behavior of various railroad steels. *J Tribol* **133**, 021602(9).
23. Herian J, Aniołek K, Cieśla M, Skotnicki G (2014) Shaping the structure during rolling and isothermal annealing, and its influence on the mechanical characteristics of high-carbon steel. *Mater Sci Eng A* **608**, 149–154.
24. Pickering FB (1975) *The Basic of Quantitative Metallography*, The Chaineleon Press Ltd., London.
25. Dequn KD, Qingsuo LQ, Yuan L (2014) Effect of austenitizing temperature on formation of hard bainite. *Met Sci Heat Treat* **56**, 444–448.
26. Ghassemi-Armaki H, Maaβ R, Bhat SP, Sriram S, Greer JR, Kumar KS (2014) Deformation response of ferrite and martensite in dual phase steel. *Acta Mater* **62**, 197–211.
27. Li G, Hong Z, Yan Q (2015) The influence of microstructure on the rolling contact fatigue of steel for high-speed-train wheel. *Wear* **342–343**, 349–355.
28. Hua J, Pan J, Liu P, Zhang G, Wu S, Chen C, Zhao X, Ren R (2021) EBSD study on proeutectoid ferrite and eutectoid ferrite refinement mechanism of D2 wheel steel under a rolling condition. *Tribol Lett* **69**, 148.
29. Lee KM, Polycarpou AA (2005) Wear of conventional pearlitic and improved bainitic rail steels. *Wear* **259**, 391–399.
30. Sawley K, Kristan J (2003) Development of bainitic rail steels with potential resistance to rolling contact fatigue. *Fatigue Fract Eng Mater Struct* **26**, 1019–1029.
31. Aleksandra K, Grzegorz L, Krzysztof R, Roman K, Aleksandra J, Rafał M, Tomasz Z (2021) Comparison of fatigue crack growth rate: Pearlitic rail versus bainitic rail. *Int J Fatigue* **149**, 106280.
32. Korda AA, Mutoh Y, Miyashita Y (2006) Effects of pearlite morphology and specimen thickness on fatigue crack growth resistance in ferritic-pearlitic steels. *Mater Sci Eng A* **428**, 262–269.
33. Garbarz B, Pickering FB (1988) Effect of pearlite morphology on impact toughness of eutectoid steel containing vanadium. *Mater Sci Technol* **4**, 328–333.
34. Zhou S, Zuo Y, Li Z, Wang X, Yong Q (2016) Microstructural analysis on cleavage fracture in pearlitic steels. *Mater Charact* **119**, 110–113.
35. Eden HC, Garnham JE, Davis CL (2013) Influential microstructural changes on rolling contact fatigue crack initiation in pearlitic rail steels. *Mater Sci Techno* **21**, 623–629.
36. Olofsson U, Telliskivi T (2003) Wear, plastic deformation and friction of two rail steels-a full-scale test and a laboratory study. *Wear* **254**, 80–93.
37. Ma L, He CG, Zhao XJ, Wang HY, Wang WJ, Zhu Y, Liu QY, Jin XS (2016) Study on wear and rolling contact fatigue behaviors of wheel/rail materials under different slip ratio conditions. *Wear* **366–367**, 13–26.
38. Li Q, Juo G, Zhao A (2019) Effect of upper bainite on wear behavior of high-speed wheel steel. *Tribol Lett* **67**, 121.
39. Stock R, Pippan R (2011) RCF and wear in theory and practice-The influence of rail grade on wear and RCF. *Wear* **271**, 125–133.
40. Pauschitz A, Roy M, Franek F (2008) Mechanisms of sliding wear of metals and alloys at elevated temperatures. *Tribol Int* **41**, 584–602.
41. Tosangthum N, Krataitong R, Wila P, Koiprasert H, Buncham K, Kansuwan P, Manonukul A, Sheppard P (2022) Dry rolling-sliding wear behavior of ER9 wheel and R260 rail couple under different operating conditions. *Wear* **518–519**, 204636.
42. Junjie F, Guifeng Z, Jianhua Z, Xudong Z, Zhao L, Duo Z, Run W (2023) Research on the effect of pearlite lamellar spacing on rolling contact wear behavior of U75V rail steel. *Metals* **13**, 237.